PHYSICAL REVIEW B **92**, 045211 (2015)

Systematic approach for simultaneously correcting the band-gap and *p*-*d* separation errors of common cation III-V or II-VI binaries in density functional theory calculations within a local density approximation

Jianwei Wang,[1] Yong Zhang,[1,*] and Lin-Wang Wang[2]
[1]*Department of Electrical and Computer Engineering, The University of North Carolina at Charlotte, 9201 University City Boulevard, Charlotte, North Carolina 28223, USA*
[2]*Materials Sciences Division, Lawrence Berkeley National Laboratory, One Cyclotron Road, Mail Stop 50F, Berkeley, California 94720, USA*

(Received 6 April 2015; revised manuscript received 2 July 2015; published 31 July 2015)

We propose a systematic approach that can empirically correct three major errors typically found in a density functional theory (DFT) calculation within the local density approximation (LDA) simultaneously for a set of common cation binary semiconductors, such as III-V compounds, (Ga or In)X with $X = \mathrm{N,P,As,Sb}$, and II-VI compounds, (Zn or Cd)X, with $X = \mathrm{O,S,Se,Te}$. By correcting (1) the binary band gaps at high-symmetry points Γ, L, X, (2) the separation of p-and d-orbital-derived valence bands, and (3) conduction band effective masses to experimental values and doing so simultaneously for common cation binaries, the resulting DFT-LDA-based quasi-first-principles method can be used to predict the electronic structure of complex materials involving multiple binaries with comparable accuracy but much less computational cost than a GW level theory. This approach provides an efficient way to evaluate the electronic structures and other material properties of complex systems, much needed for material discovery and design.

DOI: 10.1103/PhysRevB.92.045211 PACS number(s): 71.15.Dx, 71.15.Mb, 71.20.Nr

I. INTRODUCTION

A. The band gap errors in DFT-LDA calculations and their corrections

Various modeling methods based on density functional theory (DFT) have become powerful tools to explore the properties of materials [1,2]. DFT methods implemented within a local density approximation (LDA) or generalized gradient approximation (GGA) have been broadly used in ground state calculations for explaining a wide range of ground state phenomena in condensed matter physics, despite their enduring deficiency in describing exchange and correlation energies and the lack of derivative discontinuity in their exchange-correlation functional [1]. The best-known consequence of this deficiency is perhaps that the LDA tends to underestimate the band gap in semiconductors and insulators, compared with experimental results [3]. It also affects valence band properties, such as the energy separation of the valence bands derived from p orbitals and highly localized d orbitals [4]. Many different alternative methods have been developed to address this problem [3,5–21], most famously a many-body perturbation GW method which is capable of reproducing the experimental band gaps of common semiconductors to within 0.1–0.3 eV [18–21]. However, the GW method is computationally very expensive, and sometimes suffers from the conduction band cutoff convergence problem [22]. Although it is now possible to use a GW method to calculate systems up to 100 atoms [23], it is still difficult to calculate systems much larger than that, e.g., a 1000-atom nanostructure. It is thus beneficial to have DFT methods which require only the LDA level computational effort, but can predict the electronic structure accurately. For many practical problems, we encounter new systems that are heterostructures built upon two or more well-studied binaries, for instance, in the form of an alloy or a superlattice that involves a structural unit much larger than a GW method can calculate. Examples may include quarternary alloys like GaAsSbN for applications in multijunction solar cells, IR detection and emission [24,25]. And highly lattice-mismatched ZnO-ZnSe core-shell nanowires for photovoltaic (PV) application [26]. For some structurally simpler but large structures, for instance, binary quantum dots and wires or ternary alloys, some DFT-LDA-based techniques incorporating atomistic level empirical corrections to the atomic pseudopotentials have been shown able to yield rather satisfactory results for selected properties ranging from structural properties (in the DFT-LDA level) to electronic and optical properties (after applying the empirical correction, DFT-LDA-C, C stands for "corrections") [27–34]. In certain cases, a DFT-LDA-C method can often offer very good results for the electronic structure, with accuracy comparable to that of optical spectroscopy (typically on the order of 10 meV) [35–38] Besides the electronic structure, this type approach has also been shown to yield significantly better results in calculating the ground state properties (e.g., binary formation energy) [39]. However, it remains impractical to calculate more complex structures that involve more than two binaries and correct LDA errors in more than just the band gap (see more discussion later). Thus, a systematic correction to the DFT method can provide a powerful tool for accurate material simulations and material discovery.

B. Empirical methods and comparison with DFT

The empirical methods, especially a $\mathbf{k}\cdot\mathbf{p}$ method [40], often show some advantages over the first-principles methods in accuracy when using them to describe the bulk electronic structure, when the necessary input parameters are available experimentally. Based on the $\mathbf{k}\cdot\mathbf{p}$ perturbation theory, a limited set of parameters (for example, the Luttinger parameters $\gamma_1,\gamma_2,\gamma_3$ and the electronic effective mass m^*) are used to fit

---

[*] yong.zhang@uncc.edu

the experimentally determined dispersions of the conduction bands and valence bands. Such fitting usually can give very accurate descriptions of the experimentally derived bulk band structures near high-symmetry points of the Brillouin zoon (BZ). More significantly, the fitting parameters can often be used for predicting heterostructures consisting of the relevant bulk materials, for instance, a superlattice. The success of the **k**·**p** theory lies in that the symmetry of the band structure is correctly described by a set of symmetry operators, where the relevant coefficients can be determined empirically. These coefficients are otherwise difficult to obtain with high accuracy through direct first-principles calculations. Of course, a **k**·**p**-based theory has its major limitation in dealing with the situation where atomistic scale structure modification becomes important. The success of various non-self-consistent atomistic methods is in fact in the same spirit, although implicitly, in particular in a tight-binding approach [41]. An empirical pseudopotential method (EPM) can actually predict the electronic structure of a semiconductor alloy with an accuracy in the order of 10 meV, when the atomic pseudopotentials for binaries are accurately obtained [42]. However, such a non-self-consistent method is incapable of predicting the structure of the material and dealing with interatomic charge transfer. Therefore, it is highly desirable to have a DFT-LDA-C method that incorporates empirical corrections in the atomistic level to mitigate the LDA band gap errors. As a matter of fact, there have been a number of approaches proposed in the literature along this line, including one that has been used by some of us in recent years [27], that is, after performing the self-consistent calculation, empirical corrections to the *s*, *p*, and *d* components of atomistic pseudopotentials are introduced to fit the major band gaps of the binaries to the experimental values. This approach has been shown to work very well, often with a few meV accuracy, in determining the impurity levels and alloy band gaps [35–37]. However, in the past, the fitting was typically done case by case for two binaries with a common cation, for instance, GaP and GaN or GaAs and GaN, where the corrections to Ga pseudopotentials were different for the two pairs. Thus, for each new heterostructure binary pair, a new fitting will be needed. Furthermore, to correct the LDA error in the effective mass, a different set of the parameters, which might not necessarily be able to also yield satisfactory band gaps, would be required [28]. This situation limits the applicability of this method to more complex structures, not to mention non-common-cation structures. In addition, the LDA error in the valence band *p*-*d* separation was not corrected, which could affect the accuracy in the description of the valence band and related impurity or defect states.

In this work, we develop a systematic approach that allows us to generate a single set of *s*, *p*, and *d* atomistic pseudopotential corrections for a given cation, e.g., Zn, that works almost equally well with different anions of the same group: O, S, Se, Te, that can simultaneously correct band gaps of the most important critical points (Γ, *L*, and *X*) and the valence band *p*-*d* separation. This method is also applicable and usually sufficient to treat a non-common-cation system, because the corrections for the anions can be realized by taking a weighted average based on their coordination number with different cations, as done in the EPM [42]. With this approach, one may be able to predict the electronic structure with the GW level accuracy or even better for any superstructures involving, for instance, (Zn or Cd)X ($X =$ O,S,Se,Te) with only the computational effort of the LDA. Note that simultaneous fitting of multiple binaries not only allows us to deal with more complex structures but also applies more constraint to the parameters and reduces the ambiguity and potentially improves the transferability to other materials. Furthermore, once the energy levels of the critical points are correctly determined, we expect that the correct dispersion relations in the whole BZ should also follow naturally, for instance, the effective masses. The approach is also applicable to most commonly encountered III-V binaries: (Ga or In)X ($X=$ N,P,As,Sb), with the possibility of including more elements. In a nutshell, our approach is in the

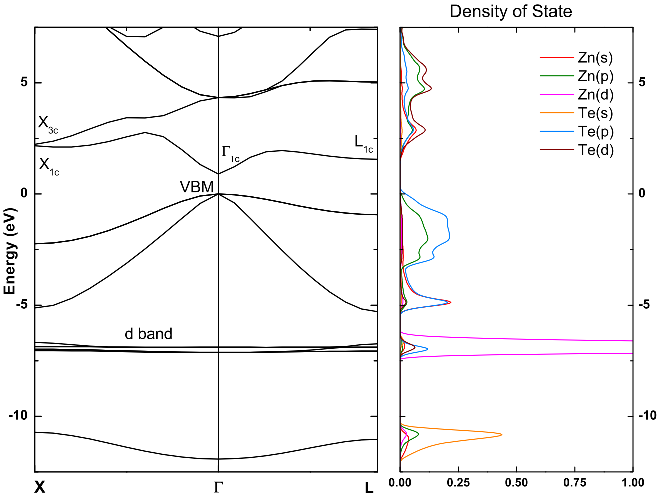

FIG. 1. (Color online) The electronic structure (left) and partial density of states (right) for zinc-blende ZnTe from a DFT-LDA calculation without spin-orbit coupling.

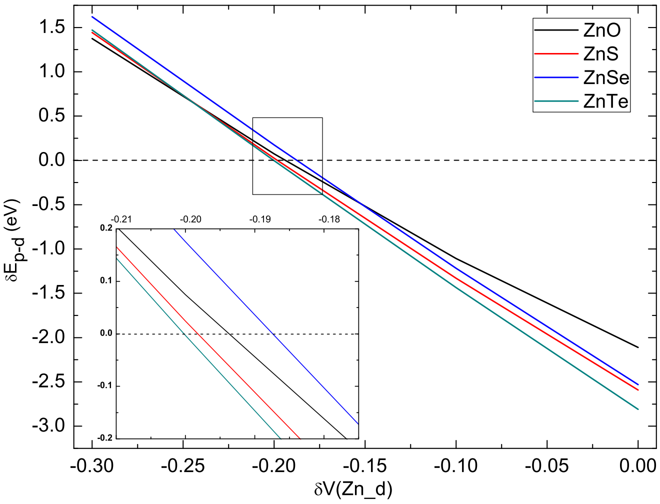

FIG. 2. (Color online) The deviation of the p-d separation $\delta E_{p\text{-}d}$, $\delta E_{p\text{-}d} = E_{p\text{-}d}(\text{cal.}) - E_{p\text{-}d}(\text{expt.})$, vs. δV(Zn_d) for ZnO, ZnS, ZnSe and ZnTe. The inset shows an enlarged view for the δV(Zn_d) region where $\delta E_{p\text{-}d}$ approaching zero.

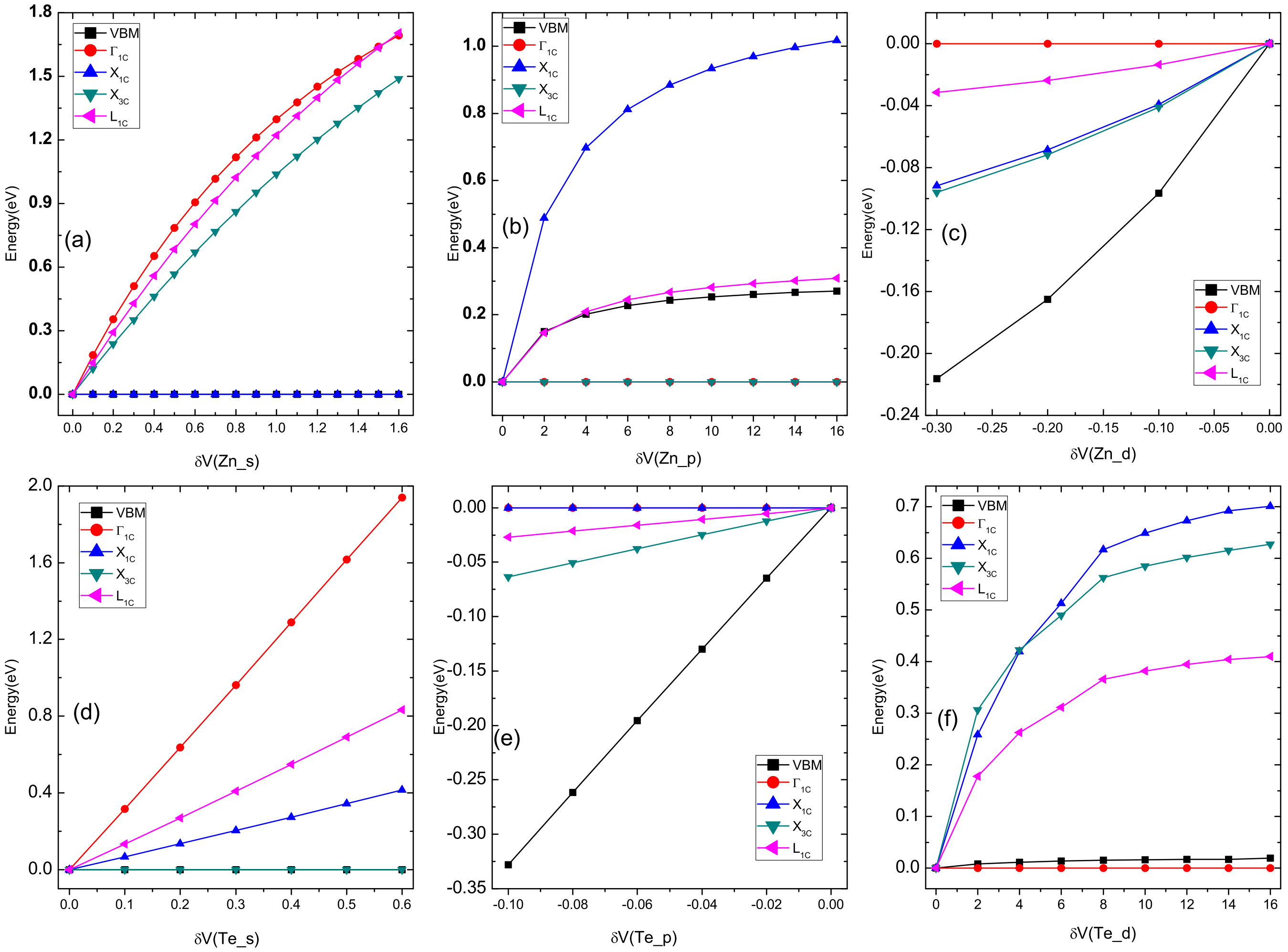

FIG. 3. (Color online) Shifts of energy levels (VBM, Γ_{1c}, X_{1c}, X_{3c}, and L_{1c}) vs. fitting parameters of six orbitals (s, p, and d orbitals of Zn atom and Te atom).

same spirit of the $\mathbf{k}\cdot\mathbf{p}$ theory but at an atomistic level, because the electronic states of different high-symmetry $\mathbf{k}$ points are related by the symmetry operations of the system and can be determined by a small set of parameters that can be more conveniently derived experimentally. In the meantime, the conventional DFT-LDA or GGA methods can be used for computing the ground state properties of the system.

II. COMPUTATIONAL METHODS

A. DFT-LDA calculations

A plane wave pseudopotential code PETOT [43] is used for the binary band structure calculation in the LDA with norm-conservation pseudopoentials. The exchange-correlation contribution is accounted for by means of Perdew and Zunger's parametrization of the calculations by Ceperley and Alder [44]. The *d* electrons are included as valence electrons for cation atoms. The special $\mathbf{k}$ points are generated using an $8 \times 8 \times 8$ mesh, which generates 60 special $\mathbf{k}$ points in the first BZ. The spin-orbit coupling is included using the ESCAN code [45]. The experimental lattice constants are used. The kinetic energy cutoff has been tested and chosen to be 60 Ry. The semiconductors considered here are all in the zinc blende (ZB) structure, even though some may prefer to crystallize in wurtzite phase in the normal growth conditions.

In our approach, a local correction term is added to each of the *s*, *p*, and *d* nonlocal pseuduopentials to fit the band gaps at high-symmetry points of the BZ (e.g., Γ, *X*, and *L* points in the ZB structure) [27]. In the past, we fitted only the band gaps involving these states: Γ_{8v}, Γ_{1c}, X_{1c}, X_{3c}, and L_{1c} of the ZB structure, while keeping the LDA valence band maximum (VBM) fixed (no net change). However, a major portion of the band gap error in the LDA can be due to the *p*-*d* valence band separation $E_{p\text{-}d}$ being too small, which causes too strong *p*-*d* repulsion that pushes up the VBM. This effect is well known to be critically important for getting the correct band gap for some binaries (e.g., ZnO), as well as in describing the band offset between two binaries. Thus, in this work, we introduce a correction to the cation *d* orbital to adjust the *p*-*d* separation to match the experimentally measured values.

B. Procedures for making band gap corrections

The method described here is still a post-treatment in order to produce accurate band structure. A self-consistent

TABLE I. LDA-corrected spin-orbit coupling Δ_{SO}, p-d separation $E_{p\text{-}d}$, and energy levels at special **k** points $\Gamma_{1c}, X_{1c}, X_{3c}$, and L_{1c} for ZnX(X = O, S, Se, and Te) and CdX(X = S, Se, and Te). Numbers in parentheses (), braces {}, and square brackets [] denote the experimental values, quasiparticle (GW) calculation results, and original LDA calculation results without the corrections, respectively.

	a (Å)	Δ_{SO} (eV)	$E_{p\text{-}d}$ (eV)	Γ_{1c} (eV)	X_{1c} (eV)	X_{3c} (eV)	L_{1c} (eV)
ZnO	4.620[a]	−0.005	7.513	3.394	8.316	10.384	7.782
		(−0.004[b])[c]	(7.5[d])	{3.394[e]}	{8.199[e]}	{10.998[e]}	{8.449[e]}
		[−0.032]	[5.381]	[0.521]	[5.176]	[8.416]	[5.131]
ZnS	5.409[f]	0.067	8.985	3.800	5.182	5.460	5.156
		(0.067[b])	(9.03[g])	(3.80[f])	{5.14[f]}	{6.03[f]}	{5.28[f]}
		[−0.054]	[6.560]	[1.751]	[3.183]	[3.868]	[3.006]
ZnSe	5.668[f]	0.404	9.305	2.82	4.428	4.452	4.153
		(0.400[b])	(9.20[g])	(2.82[f])	{4.41[f]}	{5.01[f]}	{4.14[f]}
		[0.348]	[6.787]	[0.960]	[2.704]	[3.191]	[2.234]
ZnTe	6.089[f]	0.986	9.765	2.398	3.364	3.670	3.188
		(0.970[b])	(9.84[g])	(2.39[f])	{3.47[f]}	{3.53[f]}	{3.07[f]}
		[0.902]	[7.323]	[0.609]	[1.877]	[1.943]	[1.273]
CdS	5.818[f]	0.051	9.737	2.552	5.196	5.725	4.675
		(0.067[h])	(9.64[g])	(2.55[f])	{5.08[f]}	{6.17[f]}	{4.82[f]}
		[0.051]	[7.776]	[0.832]	[3.277]	[4.141]	[2.720]
CdSe	6.052[f]	0.417	10.027	1.901	4.419	4.673	3.788
		(0.416[h])	(10.04[g])	(1.90[f])	{4.37[f]}	{5.20[f]}	{3.87[f]}
		[0.400]	[8.125]	[0.270]	[2.785]	[3.476]	[2.064]
CdTe	6.480[f]	0.926	10.402	1.603	3.511	3.658	2.993
		(0.920[h])	(10.49[g])	(1.60[f])	{3.46[f]}	{3.64[f]}	{2.84[f]}
		[0.879]	[8.570]	[0.140]	[2.144]	[2.280]	[1.299]

[a] Reference [48].
[b] Reference [50].
[c] Δ_{SO} (wurtzite).
[d] Reference [52].
[e] Reference [71].
[f] Reference [49].
[g] Reference [4].
[h] Reference [51].

calculation is performed first to generate the charge density and local potential.

There are six s, p, and d atomic orbitals available for a given binary in fitting. If we want to fit, for instance, ZnX (X= O,S,Se,Te) with the same set of Zn orbitals, there will be fewer adjustable parameters. It is important to have a general insight as to how different orbitals affect energy levels at special **k** points. We first briefly review the impact of each orbital on the energy levels of the high-symmetry points of interest. Figure 1 shows the calculated band structure of ZnTe in the LDA, together with the projections of the s, p, and d densities of states (DOSs). The d bands (one triplet $d_{3/2}$ and one doublet state $d_{1/2}$ without spin-orbit coupling, or two doublet and one singlet state with spin-orbit coupling) are located very close to each other and form a band, which is referred to as the d band. The width of the d band is usually in the range of several hundreds of meV. The center of the d band is used to calculate the p-d separation $E_{p\text{-}d}$ where the p energy level is taken from the top of valence band.

Comparing the energy levels with the projected DOSs, the d component of Zn in the DOS is far greater than others at the center of the d band. This suggests that the d band mainly comes from the d orbital of Zn. There are some components coming from other orbitals near the center of the d band, for instance, the second major component is the p orbital of Te, which reflects the p-d coupling. This information suggests the first step of the action should be adjusting the d orbital of the Zn atom to make the calculated $E_{p\text{-}d}$ match the corresponding experimental value. Figure 2 plots $\delta E_{p\text{-}d}$ vs $\delta V(\text{Zn\_}d)$ for the four binaries, where $\delta E_{p\text{-}d} = E_{p\text{-}d}(\text{calc.}) - E_{p\text{-}d}(\text{expt.})$ is the deviation of $E_{p\text{-}d}$ relative to its experimental value, and $\delta V(\text{Zn\_}d)$ is the amplitude of local potential added to the d component of the Zn pseudopotential. It can be seen from Fig. 2 that $\delta E_{p\text{-}d}$ can be tuned from −2.81 eV to 1.47 eV when $\delta V(\text{Zn\_}d)$ varies from 0.0 to −0.3. We note that the $\delta V(\text{Zn\_}d)$ value that yields the best correction (i.e., $\delta E_{p\text{-}d} = 0$) varies only slightly from one binary to the other, as shown in the inset of Fig. 2; the values are −0.194, −0.198, −0.188, and −0.200, respectively, for ZnO, ZnS, ZnSe, and ZnTe. Therefore, we can achieve very good fitting of $E_{p\text{-}d}$ for all ZnX(X= O,S,Se, and Te) by simply taking the average value of $\delta V(\text{Zn\_}d)$. The corresponding errors of $E_{p\text{-}d}$ are merely 12, 45, 105, and 75 meV for ZnO, ZnS, ZnSe, and ZnTe, respectively. The largest error is 105 meV for ZnSe, which is negligible compared to $E_{p\text{-}d}$ of 9.20 eV. It is interesting and important to find that a common value $\delta V(\text{Zn\_}d) = -0.195$ can simultaneously correct $E_{p\text{-}d}$ for all the binaries with deviations comparable to the uncertainty of the experimental

TABLE II. LDA-corrected spin-orbit coupling Δ_{SO}, p-d separation $E_{p\text{-}d}$, and energy levels at special **k** points Γ_{1c}, X_{1c}, X_{3c}, and L_{1c} for GaX(X= N, P, As, and Sb) and InX(X= P, As, and Sb). Numbers in parentheses (), braces {}, and square brackets [] denote the experimental values, quasiparticle (GW) calculation results, and original LDA calculation results without the corrections, respectively.

	a (Å)	Δ_{SO} (eV)	$E_{p\text{-}d}$ (eV)	Γ_{1c} (eV)	X_{1c} (eV)	X_{3c} (eV)	L_{1c} (eV)
GaN	4.50[a]	0.009	17.441	3.305	4.703	7.807	6.304
		0.015[a]	(17.0[b])	(3.302[c])	{4.7[d]}	{8.4[d]}	{6.2[d]}
		[0.016]	[13.810]	[1.678]	[3.308]	[6.525]	[4.469]
GaP	5.409[e]	0.075	18.446	2.871	2.413	2.425	2.706
		(0.080[f])	(18.55[g])	(2.869[h])	(2.350[i])	(2.75[i,j])	(2.64[j])
		[0.102]	[14.711]	[1.456]	[1.474]	[1.644]	[1.404]
GaAs	5.6533[k]	0.345	18.657	1.520	1.989	2.099	1.869
		(0.340[f])	(18.9[g])	(1.519[f])	(1.98[l,m])	(2.30[m])	(1.81[m])
		[0.336]	[14.976]	[0.346]	[1.352]	[1.480]	[0.828]
GaSb	6.089[n]	0.765	18.890	0.814	1.778	1.259	1.092
		(0.752[o])	(19.0[g])	(0.8102[o])	(1.66[m])	(1.43[m])	(1.09[m])
		[0.663]	[15.284]	[−0.348]	[0.624]	[0.943]	[0.068]
InP	5.818[n]	0.060	16.902	1.439	2.440	2.639	2.200
		(0.108[f])	(16.80[g])	(1.4236[f])	{2.58[j]}	{3.08[j]}	{2.03[j]}
		[0.121]	[14.372]	[0.352]	[1.568]	[2.062]	[1.200]
InAs	6.052[k]	0.387	17.015	0.419	2.100	2.430	1.604
		(0.380[p])	(17.09[g])	(0.418[p])	{2.01[j]}	{2.50[j]}	(1.55[j])
		[0.418]	[14.097]	[−0.051]	[1.405]	[1.887]	[0.720]
InSb	6.480[f]	0.839	17.262	0.237	1.378	2.005	1.018
		(0.810[p])	(17.29[g])	(0.2352[f,p])	{1.50[j]}	{1.57[j]}	(0.89[q])
		[0.803]	[14.908]	[−0.728]	[0.996]	[1.001]	[0.102]

[a] Reference [53].
[b] Reference [60].
[c] Reference [62].
[d] Reference [64].
[e] Reference [54].
[f] Reference [57].
[g] Reference [61].
[h] Reference [63].
[i] Reference [65].
[j] Reference [68].
[k] Reference [55].
[l] Reference [66].
[m] Reference [67].
[n] Reference [56].
[o] Reference [58].
[p] Reference [59].
[q] Reference [69].

data. This adjustment of p-d separation is very similar to the treatment of p-d coupling in the LDA-1/2 method [46], where a trimmed self-energy potential derived from cation d states is added to get an improved band gap.

After the $\delta V(\mathrm{Zn\_}d)$ correction is applied, the VBM values of ZnX(X= O,S,Se,Te) are lowered by 550, 284, 227, 162 meV, respectively. Here the lowering is with respect to the core levels (i.e., the VBM becomes closer to the core levels). On one hand, the $E_{p\text{-}d}$ error contributes significantly to the LDA errors in the band gaps; on the other hand, the dependence of the VBM error on anion type also significantly affects the band offsets among these common cation binaries. Once this step is done, no further adjustment will be made to this parameter in the future steps of correcting other band gaps, and this adjusted VBM will be viewed as the correct and final one which should be kept with as little net change as possible after applying other subsequent correction steps. This new VBM is used as the reference energy level for the targeted conduction band energy levels at special **k** points according to their experimental values or GW calculation results when reliable experimental data are not available. When the spin-orbit coupling is included, one-third of the spin-orbit coupling Δ_{SO} should be added to the above-mentioned VBM.

How the other energy levels are determined by the different orbitals is complicated because of the presence of different couplings, such as s-p and p-d coupling. We continue to use ZnTe as an example to examine the effects of each individual pseudopotential component. Figure 3 shows the effects of changing all the six components on five energy levels: VBM and conduction Γ_{1c}, X_{1c}, L_{1c}, and X_{3c}. The VBM state mainly comes from the Te p orbital, but is also affected significantly by the Zn d and p orbitals, and slightly by the Te d orbital,

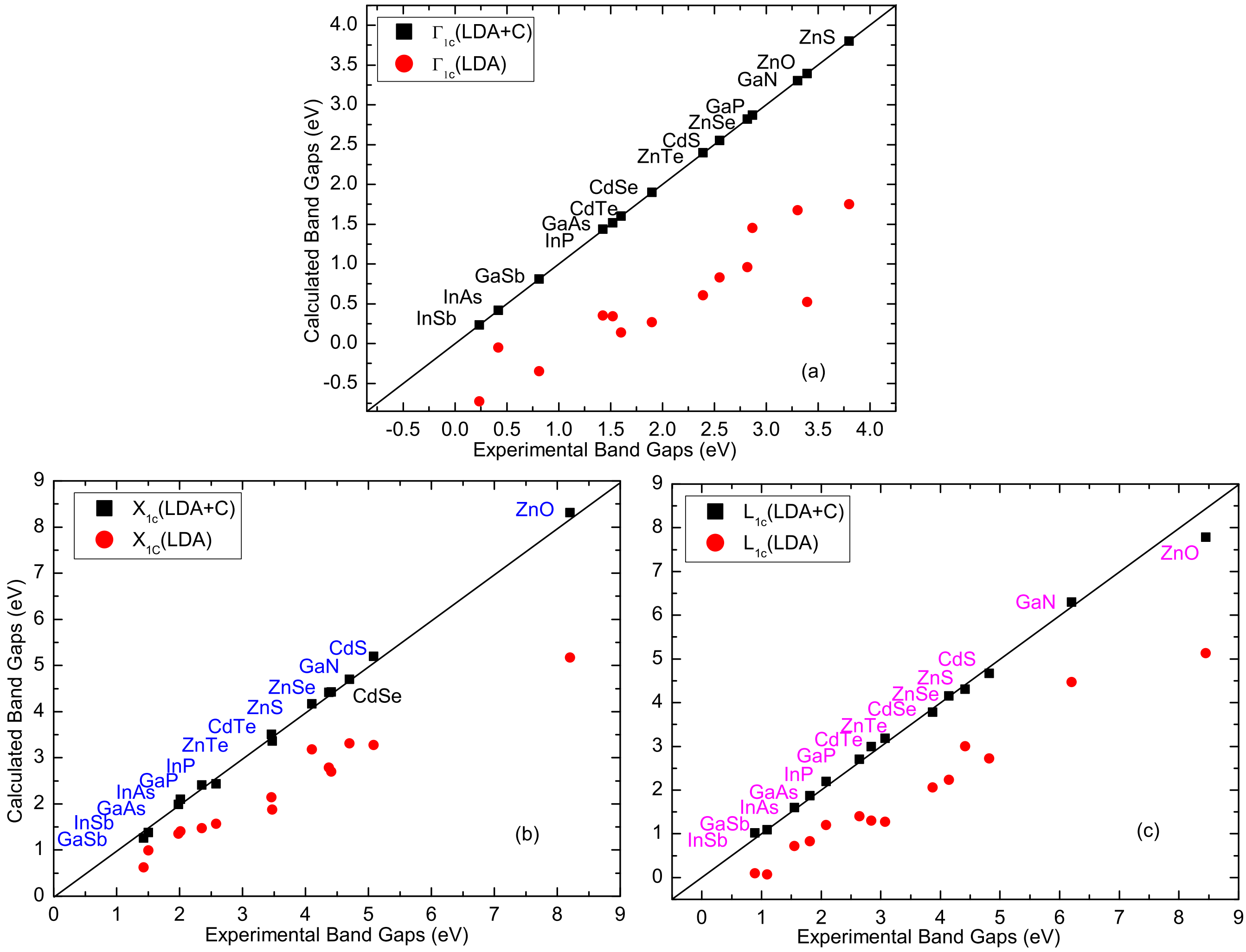

FIG. 4. (Color online) A comparison of experimental band gaps with those calculated with LDA and LDA + C methods.

which is confirmed by Figs. 3(e), 3(c), 3(b), and 3(f). The conduction band minima (CBMs) at different **k** points exhibit different dependences on the atomic orbitals: Γ_{1c} is affected by both $\delta V(\mathrm{Te}\_s)$ and $\delta V(\mathrm{Zn}\_s)$; X_{1c} by $\delta V(\mathrm{Zn}\_p)$, $\delta V(\mathrm{Zn}\_d)$, $\delta V(\mathrm{Te}\_s)$, and $\delta V(\mathrm{Te}\_d)$, but not by $\delta V(\mathrm{Zn}\_s)$ and $\delta V(\mathrm{Te}\_p)$; L_{1c} is affected by all six components, although only very weakly by $\delta V(\mathrm{Zn}\_d)$ and $\delta V(\mathrm{Te}\_p)$; and X_{3c} depends on $\delta V(\mathrm{Zn}\_s)$, $\delta V(\mathrm{Zn}\_d)$, $\delta V(\mathrm{Te}\_p)$, and $\delta V(\mathrm{Te}\_d)$, but not on $\delta V(\mathrm{Zn}\_p)$ and $\delta V(\mathrm{Te}\_s)$. Note that the fitting of $E_{p\text{-}d}$ has some minor effects on the conduction band, specifically on X_{1c}, L_{1c}, and X_{3c}, as shown in Fig. 3(c).

Our general goal here is to adjust the four conduction band states Γ_{1c}, X_{1c}, L_{1c}, and X_{3c} to obtain correct band gaps with respect to the VBM without causing further net change in the VBM, using the five remaining pseudopotential components. One way to do it would be by performing a least-squares fitting using the curves produced in Fig. 3. However, we have developed an interactive three-step procedure that usually works better. First, we note that the effects of $\delta V(\mathrm{Te}\_d)$ on X_{1c} and X_{3c} and of $\delta V(\mathrm{Zn}\_p)$ on X_{1c} tend to saturate after certain values, but the corrections are still not enough. So we adopt a value close to the saturation point for each of these two variables. Second, since the previous step has changed the VBM due to $\delta V(\mathrm{Zn}\_p)$, we use $\delta V(\mathrm{Te}\_p)$ to bring it back. Third, we use the two leftover parameters $\delta V(\mathrm{Zn}\_s)$ and $\delta V(\mathrm{Te}\_s)$ to get Γ_{1c} and X_{1c} to the targeted values, and in the meantime the separation of X_{3c} and X_{1c} close to the targeted value as well. Usually, the experimental value for the X_{3c} is less well known and its value is also less critical to the properties of interest; we put more weight on Γ_{1c} and X_{1c}. L_{1c} is not explicitly included in these steps, but typically turns out to be fairly close to the targeted value, which can be taken as an indicator for the success of this procedure. We note that the exact order of these steps is not critical.

The procedure described above allows us to perform LDA corrections for the whole set of binaries with a common cation, in this case, ZnX (X= O,S,Se,Te). The same correction parameters for the three components of the Zn pseudopotential are shared by all the Zn-based binaries. We also apply this approach to Cd-based II-VI compounds, and Ga- and In-based III-V compounds. The corrected results are described in the following section, and all the fitting parameters are given in the Appendix. The original (generated by the PETOT package

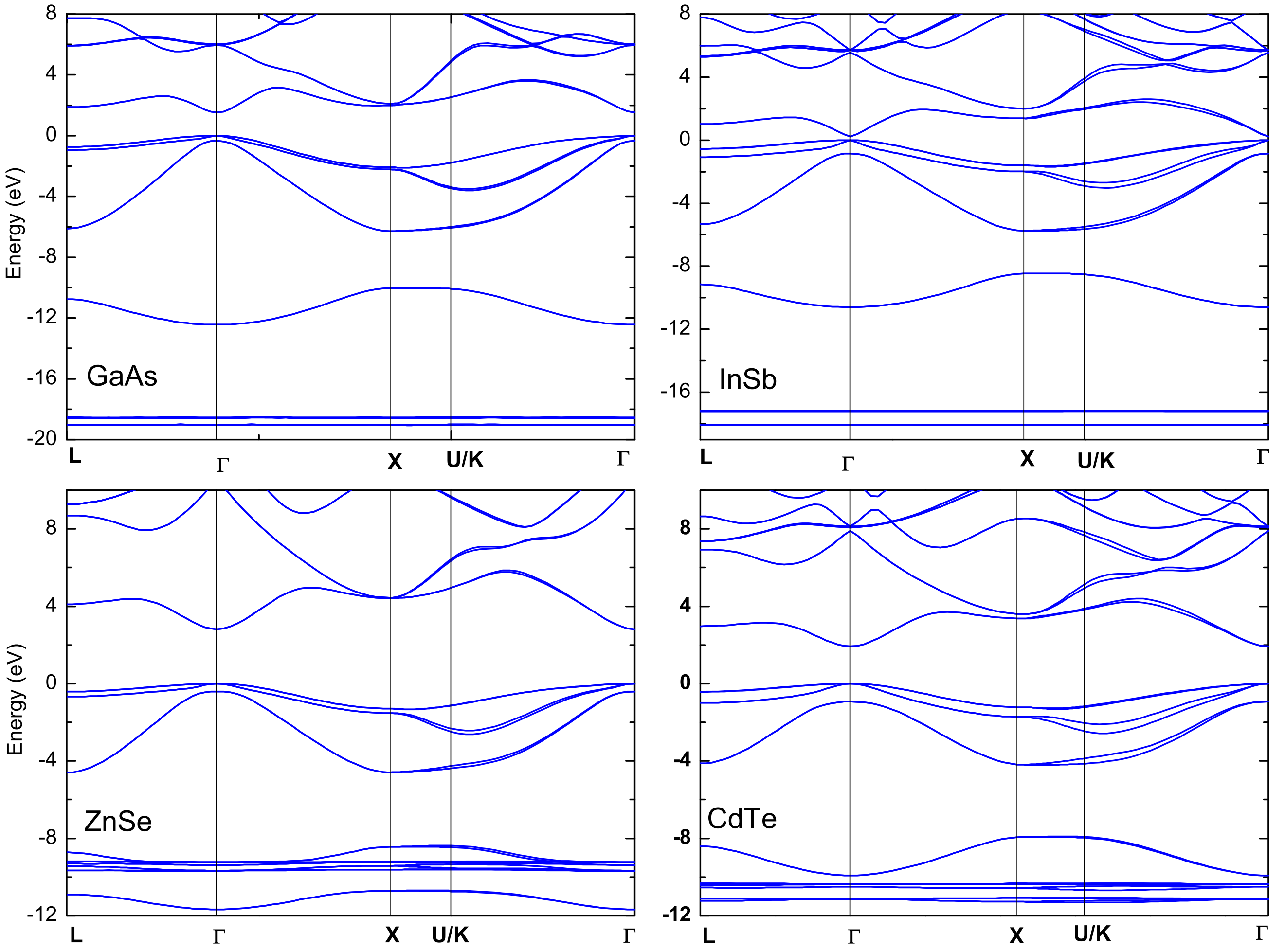

FIG. 5. (Color online) Band structures of GaAs, InSb, ZnSe, and CdTe.

[43]) and corrected pseudopotentials are available on our group website [47] or can be provided upon request.

III. RESULTS AND DISCUSSION

Listed in Table I are the LDA-corrected results of spin-orbit coupling, *p-d* separation, and energy levels of Γ_{1c}, X_{1c}, X_{3c} and L_{1c} for group II-VI semiconductors with Zn and Cd as the cation. Table II contains the same results for group III-V semiconductors with Ga and In as the cation. Overall, these corrected values are at least as good if not better than what have been achieved before either by applying other empirical correction schemes or using the GW method, in particular, done simultaneously for multiple common cation compounds.

The corrected Γ_{1c} band gaps are typically within a few meV of the targeted values for all binaries. For an indirect band gap material like GaP with its CBM at the X point, the deviation is only 63 meV from its experimental value. The comparisons between the raw LDA, LDA-corrected, and experimental or targeted band gaps for Γ_{1c}, X_{1c}, and L_{1c} are compiled in Fig. 4. The electronic band structures are plotted in Fig. 5 for selected compounds GaAs, InSb, ZnTe, and CdTe.

Besides the band gaps at the special **k** points, we further test the ability of the correction scheme to generate accurate dispersion curves, specifically the effective mass. The electron effective masses along the [001] direction are calculated and compared with available experimental or calculation results, tabulated in Table III. The agreements are remarkably good. The ability to also yield accurate effective masses further affirms the success and reliability of this correction scheme,

TABLE III. Effective mass of electrons for III-V and II-VI semiconductors (in units of the electron free mass m_0) calculated by the original LDA and the LDA + C methods are compared with their available experimental values.

	LDA	LDA + C	Expt.		LDA	LDA + C	Expt.
GaN	0.171	0.167	0.20[a]	ZnO	0.131	0.219	
GaP	0.104	0.112	0.13[a]	ZnS	0.074	0.161	0.184[b]
GaAs	0.053	0.066	0.067[a]	ZnSe	0.090	0.113	0.130[b]
GaSb	0.015	0.045	0.039[a]	ZnTe	0.068	0.102	0.130[b]
InP	0.059	0.081	0.0795[a]	CdS	0.109	0.137	
InAs	0.016	0.023	0.026[a]	CdSe	0.065	0.099	0.12[c]
InSb	0.087	0.015	0.0135[a]	CdTe	0.066	0.085	0.094[c]

[a] Reference [57].
[b] Reference [50].
[c] Reference [70].

because it is resting on sound physics based on the internal symmetry connection among different special **k** points.

Although the corrections were applied to the ZB structure, the modified pseudopotentials can be used in predicting other crystal structures. For instance, we have calculated ZnO with the wurtzite structure, and found the band gap to be 3.52 eV, which is consistent with the GW calculation and experimental results ~3.60 eV [71]. The same correction parameters can be used for more complex structures, such as superlattices and alloys. We have recently applied this method to the band structures of InAs/GaSb type-II superlattices with small band gaps of $10-100\,\text{meV}$, where the LDA calculation typically yield negative band gaps. Very good agreements with experimental results were achieved after applying the correction [38]. Based on the success of applying this approach to the InAs/GaSb superlattice, this method should be able to give more accurate band offsets than the straight DFT. However, it is beyond the scope of this work to explicitly extract the band offset values for these materials, which on its own would be a significant effort [72].

IV. CONCLUSIONS

In conclusion, we have developed a systemic approach to correct the band gap errors in DFT-LDA calculations. A reliable and easy to follow procedure is prescribed and demonstrated with great success for producing correct band structures for III-V and II-VI compounds, including the band gaps at most important critical points, *p*-*d* band separation in the valence band, and the conduction band effective mass. As a method offering atomistic level corrections to the LDA results for the ZB structure, the transferability to other related structures have been tested, yielding very good results. The ability to simultaneously correct multiple common cation binaries with the same correction parameters for the cation makes it very useful for studying complex structures with multiple anions and cations. In the future, more extensive testing will be performed for computing other band structure parameters, such as deformation potentials, and various material properties. This approach is expected to be as accurate as the GW method, sometimes even better, for many practical applications but without the demand for large computational resources.

ACKNOWLEDGMENTS

Work at UNCC was supported by the U.S. ARO/MURI Program (Grant No. Army W911NF-10-1-0524). Y.Z. acknowledges support of the Bissell Distinguished Professorship. L.W.W.'s work is supported by the Director, Office of Science, Basic Energy Science/Materials Science and Engineering Division of the U.S. Department of Energy (DOE) under the Contract No. DE-AC02-05CH11231 through the Materials Theory program. This work used computational resources at NERSC.

APPENDIX

TABLE A-I. List of cutoff radius (in unit of Bohr radius) for pseudopotentials.

	r_c		r_c		r_c
Zn_s	2.30	Zn_p	2.30	Zn_d	2.30
O_s	1.45	O_p	1.45	O_d	1.00
S_s	1.70	S_p	1.70	S_d	1.70
Se_s	1.90	Se_p	1.90	Se-d	1.90
Te_s	2.60	Te_p	2.60	Te_d	2.60
Cd_s	2.65	Cd_p	2.65	Cd_d	2.65
Ga_s	2.10	Ga_p	2.10	Ga_d	2.10
In_s	2.90	In_p	2.90	In_d	2.90
N_s	1.50	N_p	1.50	N_d	0.00
P_s	1.95	P_p	1.95	P_d	1.95
As_s	2.10	As_p	2.40	As_d	3.00
Sb_s	2.60	Sb_p	2.60	Sb_d	2.60

TABLE A-II. Fitting parameters for ZnX.

Zn_s	0.500	Zn_p	10.0	Zn_d	−0.19502525
O_s	0.652555	O_p	−0.0273929	O_d	10.0
S_s	0.640480	S_p	−0.1008	S_d	5.0
Se_s	0.568804	Se_p	−0.114591	Se_d	10.0
Te_s	0.269504	Te_p	−0.072394	Te_d	22.0

TABLE A-III. Fitting parameters for CdX.

Cd_s	0.450	Cd_p	7.00	Cd_d	−0.172982
S_s	0.621348	S_p	−0.08192	S_d	22.0
Se_s	0.574695	Se_p	−0.094994	Se_d	12.0
Te_s	0.345548	Te_p	−0.060212	Te_d	4.0

TABLE A-IV. Fitting parameters for GaX.

Ga_s	0.60	Ga_p	3.482	Ga_d	−0.252373
N_s	0.250114	N_p	−0.0348319	N_d	6.0
P_s	0.174723	P_p	−0.129255	P_d	1.29255
As_s	0.0649773	As_p	−0.0862555	As_d	0.0
Sb_s	−0.141989	Sb_p	−0.002094	Sb_d	2.0

TABLE A-V. Fitting parameters for InX.

In_s	0.20	In_p	2.0	In_d	−0.172582
P_s	0.196927	P_p	−0.119467	P_d	0.0
As_s	0.107101	As_p	−0.0833195	As_d	−0.50
Sb_s	0.0880463	Sb_p	−0.130506	Sb_d	1.0

[1] R. M. Martin, *Electronic Structure: Basic Theory and Practical Methods* (Cambridge University Press, Cambridge, 2008).
[2] W. Kohn and L. J. Sham, Phys. Rev. **140**, A1133 (1965).
[3] J. P. Perdew and A. Zunger, Phys. Rev. B **23**, 5048 (1981).
[4] S. H. Wei and A. Zunger, Phys. Rev. B **37**, 8958 (1988).
[5] I. A. Vladimir, F. Aryasetiawan, and A. I. Lichtenstein, J. Phys.: Condens. Matter **9**, 767 (1997).
[6] R. W. Godby, M. Schlüter, and L. J. Sham, Phys. Rev. B **37**, 10159 (1988).
[7] R. Asahi, W. Mannstadt, and A. J. Freeman, Phys. Rev. B **59**, 7486 (1999).
[8] A. Seidl, A. Görling, P. Vogl, J. A. Majewski, and M. Levy, Phys. Rev. B **53**, 3764 (1996).
[9] M. Städele, M. Moukara, J. A. Majewski, P. Vogl, and A. Görling, Phys. Rev. B **59**, 10031 (1999).
[10] A. Qteish, A. I. Al-Sharif, M. Fuchs, M. Scheffler, S. Boeck, and J. Neugebauer, Phys. Rev. B **72**, 155317 (2005).
[11] F. Tran and P. Blaha, Phys. Rev. Lett. **102**, 226401 (2009).
[12] Y.-S. Kim, M. Marsman, G. Kresse, F. Tran, and P. Blaha, Phys. Rev. B **82**, 205212 (2010).
[13] J. A. Camargo-Martínez and R. Baquero, Phys. Rev. B **86**, 195106 (2012).
[14] D. C. Langreth and M. J. Mehl, Phys. Rev. B **28**, 1809 (1983).
[15] J. P. Perdew, K. Burke, and M. Ernzerhof, Phys. Rev. Lett. **77**, 3865 (1996).
[16] J. Heyd, G. E. Scuseria, and M. Ernzerhof, J. Chem. Phys. **118**, 8207 (2003).
[17] J. Heyd, J. E. Peralta, G. E. Scuseria, and R. L. Martin, J. Chem. Phys. **123**, 174101 (2005).
[18] M. S. Hybertsen and S. G. Louie, Phys. Rev. B **34**, 5390 (1986).
[19] F. Aryasetiawan and O. Gunnarsson, Rep. Prog. Phys. **61**, 237 (1998).
[20] K. A. Johnson and N. W. Ashcroft, Phys. Rev. B **58**, 15548 (1998).
[21] M. Shishkin, M. Marsman, and G. Kresse, Phys. Rev. Lett. **99**, 246403 (2007).
[22] M. L. Tiago, S. Ismail-Beigi, and S. G. Louie, Phys. Rev. B **69**, 125212 (2004).
[23] J. Deslippe, G. Samsonidze, D. A. Strubbe, M. Jain, M. L. Cohen, and S. G. Louie, Comput. Phys. Commun. **183**, 1269 (2012).
[24] G. Ungaro, G. Le Roux, R. Teissier, and J. C. Harmand, Electron. Lett. **35**, 1246 (1999).
[25] T. W. Kim, K. Forghani, L. J. Mawst, T. F. Kuech, S. D. LaLumondiere, Y. Sin, W. T. Lotshaw, and S. C. Moss, J. Cryst. Growth. **393**, 70 (2014).
[26] Z. Wu *et al.*, J. Mater. Chem. **21**, 6020 (2011).
[27] L.-W. Wang, Appl. Phys. Lett. **78**, 1565 (2001).
[28] J. Li and L.-W. Wang, Phys. Rev. B **72**, 125325 (2005).
[29] J. Li and S.-H. Wei, Phys. Rev. B **73**, 041201 (2006).
[30] D. Segev, A. Janotti, and C. G. Van de Walle, Phys. Rev. B **75**, 035201 (2007).
[31] S.-H. Wei and A. Zunger, Phys. Rev. B **57**, 8983 (1998).
[32] J. Schrier, D. O. Demchenko, L. W. Wang, and A. P. Alivisatos, Nano Lett. **7**, 2377 (2007).
[33] Y. Zhang, Wang, and A. Mascarenhas, Nano Lett. **7**, 1264 (2007).
[34] N. E. Christensen, Phys. Rev. B **30**, 5753 (1984).
[35] Y. Zhang, B. Fluegel, M. C. Hanna, A. Mascarenhas, L.-W. Wang, Y. J. Wang, and X. Wei, Phys. Rev. B **68**, 075210 (2003).
[36] Y. Zhang, A. Mascarenhas, and L. W. Wang, Phys. Rev. B **74**, 041201 (2006).
[37] Y. Zhang, A. Mascarenhas, and L. W. Wang, Phys. Rev. B **71**, 155201 (2005).
[38] J. Wang and Y. Zhang, J. Appl. Phys. **116**, 214301 (2014).
[39] V. Stevanovic, S. Lany, X. Zhang, and A. Zunger, Phys. Rev. B **85**, 115104 (2012).
[40] L. C. Lew Yan Voon and M. Willatzen, *The $k\cdot p$ Method: Electronic Properties of Semiconductors* (Springer, Berlin, 2009).
[41] P. Vogl, H. P. Hjalmarson, and J. D. Dow, J. Phys. Chem. Solids **44**, 365 (1983).
[42] Y. Zhang, A. Mascarenhas, and L.-W. Wang, Phys. Rev. B **63**, 201312 (2001).
[43] http://cmsn.lbl.gov/html/PEtot/PEtot.html.
[44] D. M. Ceperley and B. J. Alder, Phys. Rev. Lett. **45**, 566 (1980).
[45] http://cmsn.lbl.gov/html/Escan/DOE-nano/pescan.htm.
[46] L. G. Ferreira, M. Marques, and L. K. Teles, Phys. Rev. B **78**, 125116 (2008).
[47] http://coefs.uncc.edu/yzhang47/.
[48] M. Oshikiri and F. Aryasetiawan, Phys. Rev. B **60**, 10754 (1999).
[49] O. Zakharov, A. Rubio, X. Blase, M. L. Cohen, and S. G. Louie, Phys. Rev. B **50**, 10780 (1994).
[50] S. Z. Karazhanov, P. Ravindran, A. Kjekshus, H. Fjellvåg, U. Grossner, and B. G. Svensson, J. Appl. Phys. **100**, 043709 (2006).
[51] P. Carrier and S.-H. Wei, Phys. Rev. B **70**, 035212 (2004).
[52] R. A. Powell, W. E. Spicer, and J. C. McMenamin, Phys. Rev. Lett. **27**, 97 (1971).
[53] S. H. Wei and A. Zunger, Appl. Phys. Lett. **69**, 2719 (1996).
[54] Y. Zhang, A. Mascarenhas, and L. W. Wang, Phys. Rev. Lett. **101**, 036403 (2008).
[55] D. A. H. Mace, D. C. Rogers, K. J. Monserrat, J. N. Tothill, and S. T. Davey, Semicond. Sci. Technol. **3**, 597 (1988).
[56] W. F. Boyle and R. J. Sladek, Phys. Rev. B **11**, 2933 (1975).
[57] I. Vurgaftman, J. R. Meyer, and L. R. Ram-Mohan, J. Appl. Phys. **89**, 5815 (2001).
[58] D. E. Aspnes, C. G. Olson, and D. W. Lynch, Phys. Rev. B **14**, 4450 (1976).
[59] K. P. Ghatak, S. Bhattacharya, S. Bhowmik, R. Benedictus, and S. Choudhury, J. Appl. Phys. **103**, 034303 (2008).
[60] C. Persson and A. Zunger, Phys. Rev. B **68**, 073205 (2003).
[61] L. Ley, R. A. Pollak, F. R. McFeely, S. P. Kowalczyk, and D. A. Shirley, Phys. Rev. B **9**, 600 (1974).
[62] G. Ramírez-Flores, H. Navarro-Contreras, A. Lastras-Martínez, R. C. Powell, and J. E. Greene, Phys. Rev. B **50**, 8433 (1994).
[63] S. E. Stokowski and D. D. Sell, Phys. Rev. B **5**, 1636 (1972).
[64] A. Rubio, J. L. Corkill, M. L. Cohen, E. L. Shirley, and S. G. Louie, Phys. Rev. B **48**, 11810 (1993).
[65] J.-M. Jancu, R. Scholz, F. Beltram, and F. Bassani, Phys. Rev. B **57**, 6493 (1998).
[66] R. W. Godby, M. Schlüter, and L. J. Sham, Phys. Rev. B **35**, 4170 (1987).
[67] S.-H. Wei and A. Zunger, Phys. Rev. B **39**, 3279 (1989).

[68] X. Zhu and S. G. Louie, Phys. Rev. B **43**, 14142 (1991).

[69] D. M. Brad and L. C. Marvin, J. Phys.: Condens. Matter **25**, 105503 (2013).

[70] O. Madelung, *Semiconductors: Data Handbook* (Springer, Berlin, 2004).

[71] B.-C. Shih, Y. Xue, P. Zhang, M. L. Cohen, and S. G. Louie, Phys. Rev. Lett. **105**, 146401 (2010).

[72] Y.-H. Li, A. Walsh, S. Chen, W.-J. Yin, J.-H. Yang, J. Li, J. L. F. Da Silva, X. G. Gong, and S.-H. Wei, Appl. Phys. Lett. **94**, 212109 (2009).